Regulation of Nuclear PKA revealed by spatiotemporal manipulation of cAMP

Vedangi Sample[1,^], **Lisa M. DiPilato**[1,^], **Jason H. Yang**[2,^], **Qiang Ni**[1], **Jeffrey J. Saucerman**[2,*], and **Jin Zhang**[1,3,*]

[1]Department of Pharmacology and Molecular Sciences, The Johns Hopkins University School of Medicine, 725 N. Wolfe Street, Baltimore, MD 21205

[2]Department of Biomedical Engineering, University of Virginia, Charlottesville, VA 22908

[3]Departments of Neuroscience and Oncology, The Johns Hopkins University, School of Medicine, 725 N. Wolfe St., Baltimore, MD 21205

Abstract

Understanding how specific cAMP signals are organized and relayed to their effectors in different compartments of the cell to achieve functional specificity requires molecular tools that allow precise manipulation of cAMP in these compartments. Here we characterize a new method using bicarbonate-activatable and genetically targetable soluble adenylyl cyclase (sAC) to control the location, kinetics and magnitude of the cAMP signal. Using this live-cell cAMP manipulation in conjunction with fluorescence imaging and mechanistic modeling, we uncover the activation of a resident pool of PKA holoenzyme in the nuclei of HEK-293 cells, modifying the existing dogma of cAMP-PKA signaling in the nucleus. Furthermore, we show that phosphodiesterases (PDE) and A-Kinase Anchoring Proteins (AKAP) are critical in shaping nuclear PKA responses. Collectively, our data suggests a new model where AKAP-localized PDEs tune an activation threshold for nuclear PKA holoenzyme, thereby converting spatially distinct second messenger signals to temporally controlled nuclear kinase activity.

Cyclic AMP signaling has garnered vast interest due to its role in mediating many cellular processes across a diverse number of species. In the classic mammalian model, hormone-mediated activation of G protein coupled receptors (GPCRs) initiates a cascade of intracellular events involving the activation of G alpha stimulatory protein (Gαs) and transmembrane adenylyl cyclase (tmAC) which catalyzes the conversion of ATP to cAMP.

*Corresponding Author: Jin Zhang, PhD Department of Pharmacology and Molecular Sciences The Johns Hopkins University School of Medicine 725 N. Wolfe Street, Hunterian #307 Baltimore, MD 21205 Phone: (410)502-0173 FAX: (410)955-3023 jzhang32@jhmi.edu. *Jeffrey J. Saucerman, PhD Department of Biomedical Engineering University of Virginia Box 800759 Health System Charlottesville, VA 22908 Phone: (434) 924-5095 FAX: (434) 982-3870 jsaucerman@virginia.edu.
^These authors contributed equally

This ubiquitous second messenger then diffuses throughout the cell, binding to and activating its few known effectors: cAMP-dependent protein kinase (PKA), exchange protein directly activated by cAMP (Epac), and cyclic nucleotide gated (CNG) channels[1]. Remarkably, even with the large family of GPCRs that are coupled to its generation and the limited number of effectors that translate its signal, cAMP elicits highly specific cellular responses to external stimuli. This specificity is believed to be achieved via compartmentation of cAMP signaling[2], wherein intracellular cAMP increases in a non-uniform manner despite its fast rate of diffusion. Phosphodiesterases (PDEs), the enzymes that degrade cAMP, have been shown to be responsible, at least in part, for these heterogeneous intracellular cAMP dynamics[3]. Subcellular cAMP signaling domains are further defined by the distinct environments within cellular organelles as well as the assembly of signaling complexes at intracellular sites via scaffolding proteins such as A Kinase Anchoring Proteins (AKAPs)[4].

The nucleus, for instance, defines a unique cAMP-PKA signaling domain where PKA plays important roles in regulating transcription[5] and RNA splicing[6]. The dogma of cAMP-PKA signaling in the nucleus states that, upon cAMP-induced activation of the cytosolic tetrameric PKA holoenzyme, the catalytic subunit (cat) dissociates from the regulatory subunit in an isoform-specific manner[7] and translocates into the nucleus via diffusion[8], serving as the only functional nuclear PKA species[1,5,9]. Contradictory to this dogma, the existence of an additional resident pool of nuclear PKA holoenzyme has been proposed. For example, immunoblotting and immunostaining studies have revealed the presence of PKA regulatory and catalytic subunits in the nuclei of different cell types[10,11]. Furthermore, a recent study identified a splicing factor (SRFS17A) as a nuclear localized dual-specific AKAP and showed that it requires the presence of the regulatory subunit of PKA to regulate alternative splicing[12], suggesting the involvement of a nuclear PKA holoenzyme. However, the existence of the nuclear PKA holoenzyme has not been unequivocally proven, partly due to lack of data on cellular responses resulting from the activation of such a pool of nuclear PKA holoenzyme.

In this study, we characterize a versatile system for precisely manipulating the location, kinetics and magnitude of intracellular cAMP signal via activation of soluble AC (sAC). By combining this approach with real-time imaging of cAMP and PKA dynamics as well as mechanistic modeling, we investigated the regulation of nuclear cAMP-PKA signaling. This has led to the identification of a functional pool of PKA holoenzyme in the nucleus. We further observed that cAMP generated at the plasma membrane seemed incapable of activating this nuclear pool of PKA holoenzyme unless PDE activity was inhibited or PKA anchoring via AKAP was blocked, suggesting a model where an AKAP assembles PDEs and PKA to form a signaling complex in the nucleus thereby controlling local cAMP levels and nuclear PKA activity. Thus the existence and distinct regulation of PKA holoenzyme in the nucleus depicts a complex nuclear signaling domain for processing specific cAMP signals.

Results

Spatiotemporal Manipulation of Intracellular cAMP

To better study the functional response of cAMP in distinct cellular compartments such as the nucleus, we set out to establish a system for generating intracellular cAMP with tight control of spatial and temporal parameters. Towards this end, we chose to utilize an isoform of adenylyl cyclase, soluble adenylyl cyclase (sAC), which is sensitive to a chemical activator, bicarbonate ($NaHCO_3$). This anion activates sAC by inducing active site closure and metal recruitment which results in substrate turnover[13]. In this system which we dubbed SMICUS (Spatiotemporal Manipulation of Intracellular cAMP Using sAC), a truncated, catalytically active form of sAC (sAC_t)[14,15] is the functional unit for producing cAMP. A monomeric red fluorescent protein, mCherry, is attached to the carboxy terminus of sAC_t as a marker for transfection and a means for quantifying expression. To direct the cAMP production to a designated subcellular location, we append a targeting sequence at the C- or N- terminus of the fusion construct.

We first tested this system in the cytosol of HEK-293 cells by using a sAC_t tagged with a nuclear export signal (NES) (sAC_t-NES, Fig. 1a) and our previously published FRET-based cAMP indicator, ICUE3, to monitor cAMP production[16]. ICUE3, like other cAMP probes[17,18] reports cAMP dynamics in live cells via a cAMP-binding induced change in FRET[19]. HEK-293 cells co-expressing sAC_t-NES and ICUE3-NES were placed in bicarbonate-free imaging buffer and then treated with sodium bicarbonate ($NaHCO_3$). The addition of 15 mM $NaHCO_3$ induced an immediate ICUE3 response of $29.3 \pm 3.8\%$ (n =10) [average $\pm$ SEM; n = number of cells] which was readily reversed by replacing the bicarbonate-containing media with fresh buffer (Supplementary Results, Supplementary Fig. 1a). The kinetics of the reversal were similar to that observed previously with blocking receptor-stimulated cAMP production[19], suggesting cAMP degradation dictates the kinetics of the reversal. This observed response was dependent on sAC_t, as the addition of KH7, a sAC specific inhibitor, also reversed the response (Supplementary Fig. 1b). To determine if the cAMP signal is translated into a functional response of downstream effectors, we probed PKA dynamics by using A Kinase Activity Reporter (AKAR). This reporter serves as a surrogate substrate of PKA and reports changes in PKA activity by phosphorylation-dependent changes in FRET[20]. Upon bicarbonate stimulation of HEK-293 cells co-expressing sAC_t-NES and AKAR-NES, the cytosolic reporter showed an immediate and robust response of $19.3 \pm 2.8\%$ (n = 5) with a $t_{1/2}$ of 0.9 ± 0.1 min (Fig. 1b). PKA activity was sustained in the presence of 15 mM $NaHCO_3$ and reversed immediately upon washout, demonstrating that we can manipulate not only intracellular cAMP levels but also the activity of its downstream effector in the cell.

Next, we tested the fidelity and precision of switching the system on and off by adding 15 mM $NaHCO_3$ in increasing time increments of 5, 10 and 15 minutes each followed by washout (Fig. 1c). An immediate and robust cAMP response was observed after each stimulation, and this response was sustained in the presence of bicarbonate showing no signal decay. Thus the system can be reset and stimulated again while allowing precise control of signal duration.

To further test the ability of SMICUS to tune cAMP levels, we co-expressed sAC_t-NES and ICUE3-NES in HEK-293 cells and stimulated these cells with increasing doses of $NaHCO_3$. Upon addition of a low dose of 2.5 mM $NaHCO_3$, ICUE3 gave a response of $19.3 \pm 0.02\%$ (n = 3). Subsequent doses of 2.5 mM and 7.5 mM $NaHCO_3$ resulted in step-wise increases of the cAMP levels (Fig. 1d), demonstrating that the amplitude of the cAMP signal can be tuned with specific doses of the activator.

Having characterized the system in the cytoplasm, we then generated nuclear and plasma membrane localized versions of sAC_t. We exclusively targeted sAC_t to the nucleus via a nuclear localization signal (NLS)[19] and to the plasma membrane (PM) through a lipid modification domain derived from Lyn kinase that undergoes myristoylation and palmitoylation[16]. Stimulation of HEK-293 cells co-expressing sAC_t-NLS and ICUE3-NLS with a low dose of $NaHCO_3$ produced a rapid response of $21.3 \pm 2.5\%$ emission ratio change (n = 5), and addition of subsequent doses of $NaHCO_3$ minimally affected the signal of ICUE3-NLS (Fig. 1e). On the other hand, an initial low dose of $NaHCO_3$ did not elicit a PM-ICUE3 response. Following subsequent doses of $NaHCO_3$, detectable responses were elicited suggesting that PM-ICUE3 is functional and the null response after the initial low dose of bicarbonate was due to the low level of cAMP accumulating at the plasma membrane upon stimulation of sAC_t-NLS. Similarly, when cAMP was generated at the plasma membrane via PM-sAC_t, PM-ICUE3 gave a maximal response of $11.4 \pm 0.9\%$ (n = 2) whereas the nuclearly targeted ICUE3 probe generated a relatively small response of $4.1 \pm 0.4\%$ (n = 3) (Fig. 1e), suggesting cAMP preferentially accumulated at the plasma membrane under this condition. These data demonstrate that these targeted sAC variants can be used to stimulate cAMP production locally in different subcellular compartments.

Sites of cAMP generation dictate nuclear PKA dynamics

Armed with a system for generating intracellular cAMP in designated subcellular compartments, we were interested in studying how site-specific cAMP signals are translated into nuclear PKA activity. We first monitored nuclear PKA activity upon the activation of PM-sAC_t to mimic the effect of stimulated tmACs. Addition of 15 mM $NaHCO_3$ to cells expressing PM-sAC_t and AKAR-NLS resulted in a gradual AKAR response in the nucleus (Fig. 2a) with a $t_{1/2}$ of 20.2 ± 3.0 min (n = 4), whereas a low dose of 2.5 mM $NaHCO_3$ did not induce consistent responses. The AKAR-NLS response generated by the stimulation of PM-sAC_t showed similar kinetics to that elicited by the direct activation of tmAC with forskolin (Fsk) ($t_{1/2} = 26.0 \pm 1.6$ min; n = 13) (Fig. 2b), with no statistically significant difference between the $t_{1/2}$ values of the two responses. This slow response is consistent with the rate limiting step involving the diffusional translocation of the dissociated catalytic subunit of PKA into the nucleus upon elevation of cAMP levels[8,21].

In sharp contrast, $NaHCO_3$ stimulation of either an NES- or NLS- tagged sAC_t resulted in faster AKAR-NLS responses with a $t_{1/2}$ of 3.5 ± 0.3 min (n = 9) and 4.2 ± 0.5 min (n = 7), respectively (Fig. 2). While the kinetics of nuclear PKA responses stimulated by nuclear- and cytosolic-generated cAMP are not different, these rates are significantly faster than those induced by membrane-generated cAMP via endogenous tmAC (p < 0.001 for both) or PM-sAC_t (p < 0.05 for both). To exclude the possibility that overexpression of sAC_t has

additional effects on PKA, we treated cells with Fsk in the presence of sAC_t-NLS and observed a similar AKAR-NLS response ($t_{1/2} = 29.8 \pm 2.3$ min; n = 2) to that in cells containing no sAC_t ($t_{1/2} = 26.0 \pm 1.6$ min; n = 13) (Fig. 2b). To further corroborate the fast nuclear AKAR responses induced by locally generated cAMP, we examined the phosphorylation of cAMP response element-binding protein (CREB), an endogenous substrate of PKA in the nucleus. When HEK-293 cells expressing sAC_t-NLS were stimulated with 15 mM $NaHCO_3$, we observed fast CREB phosphorylation kinetics (Supplementary Fig. 2). This fast response elicited by cAMP production in the nucleus or cytosol was surprising; it is contrary to the notion that the nuclear PKA response depends on passive diffusion of the dissociated catalytic subunit from the cytosol into the nucleus, which is characterized by slow kinetics[8]. If the PKA holoenzyme resides exclusively outside of the nucleus and nuclear translocation of the C subunit is rate-limiting[21], we would expect to see slow response kinetics of nuclear PKA activity regardless of where cAMP was generated.

Computational analysis of nuclear PKA dynamics

To more quantitatively evaluate whether the classical model is able to explain our data, we constructed a biochemically mechanistic computational model describing cAMP and PKA dynamics in the three spatial subcellular compartments (plasma membrane, cytosol, nucleus) represented in our experiments (Supplementary Fig. 3; described in detail in Supplementary Methods). This "Classical" model consists of endogenous adenylyl cyclase at the plasma membrane, PKA holoenzyme exclusively at the membrane and cytosol, and PDEs and phosphatases in all the three compartments.

We first fit this model to our plasma membrane and nuclear ICUE3 measurements generated by $NaHCO_3$ stimulation of plasma membrane and nuclear targeted sAC_t to determine if this model adequately captured cAMP dynamics (Fig. 3a, Supplementary Fig. 4 and 5). Similar to our experimental measurements, the model predicted that local ICUE3 responses saturate at lower $NaHCO_3$ doses than distal ICUE3 responses, irrespective of the location of sAC_t (Supplementary Fig. 6 and 7). Simulated ICUE3 responses have similar shape and qualitative trends, indicating the model is a good representation of both cAMP dynamics and ICUE3 activity.

To determine if the model adequately captured nuclear PKA dynamics, we simultaneously fit this model to our Fsk-stimulated cytosolic and nuclear AKAR measurements (Fig. 3b). Simulated cytosolic AKAR dynamics are fast ($t_{1/2} = 1.8$ min vs. experimental $t_{1/2} = 1.5 \pm 0.1$ min; n = 8), while simulated nuclear AKAR dynamics are slow ($t_{1/2} = 25.4$ min vs. experimental $t_{1/2} = 25.4 \pm 1.3$ min; n = 28). Confident that the Classical Model adequately described the cAMP and PKA dynamics under our experimental conditions, we simulated cytosolic PKA dynamics stimulated by $NaHCO_3$-activated cytosolic sAC_t as well as nuclear PKA dynamics stimulated by $NaHCO_3$-activated nuclear sAC_t (Fig. 3c). This model predicted rapid cytosolic PKA activation by cytosolic sAC_t ($t_{1/2} = 0.6$ min), which was qualitatively similar to the experimentally measured AKAR-NES response ($t_{1/2} = 0.9 \pm 0.1$ min; n = 5). However, under nuclear sAC_t stimulation, the model predicted slow nuclear PKA responses with a $t_{1/2} = 24.7$ min, which was in sharp contrast to the experimentally

measured AKAR-NLS kinetics ($t_{1/2}$ = 4.2 ± 0.5 min; n = 7). This identified a failure of the "Classical" model to explain the fast nuclear PKA responses.

We hypothesized that the presence of an independent pool of PKA holoenzyme in the nucleus could account for the observed fast nuclear PKA kinetics, and incorporated a nuclear PKA holoenzyme as a free parameter into the model, now termed "nucPKA Model" (Supplementary Methods). The nucPKA Model was refitted to both our targeted ICUE3 and AKAR data and predicted similar ICUE3 responses as the Classical Model (Supplementary Fig. 8). While the predictions for the PKA response kinetics in the cytosol remained relatively unchanged ($t_{1/2}$ = 0.9 min), the nucPKA Model gave a significant improvement in predicting nuclear PKA responses ($t_{1/2}$ = 6.1 min nucPKA Model vs. experimental $t_{1/2}$ = 4.2 ± 0.5 min; n = 7) (Fig. 3c).

Increasing model complexity may only trivially improve model fits to experimental data while risking increased model uncertainty. To quantitatively compare the appropriateness of selecting one model over the other, we computed the Akaike Information Criterion (AIC)[22,23] and Akaike weights for both the Classical Model (AIC = −59.12, w = 0.31) and the nucPKA Model (AIC = −60.71, w = 0.69) (Supplementary Methods). The smaller AIC value and higher Akaike weight for the nucPKA Model indicates that the nucPKA Model is a better description for the observed PKA dynamics than the Classical Model.

PKA holoenzyme is present in the nucleus

To validate this model prediction, we tested the presence of a nuclear pool of PKA holoenzyme by immunofluorescence studies using anti-pan PKA RI, anti-PKA RIIβ and anti-PKA catalytic subunit antibodies. All the three antibodies showed weak but distinct staining in the nuclei of HEK-293 cells (Fig. 4a, b), whereas staining with secondary antibodies alone did not give a signal in the nucleus (Supplementary Fig. 9a). Given that nonspecific staining could contribute to the immunofluorescence signals, we isolated the nuclei of HEK-293 cells by density centrifugation through a sucrose gradient and performed western blot analysis on the nuclear and non-nuclear fractions to further substantiate the existence of a PKA pool in the nucleus. These fractions were first probed with antibodies against CREB, a nuclear marker, as well as antibodies against β-Tubulin and glyceraldehyde 3-phosphate dehydrogenase (GAPDH) as cytosolic markers. The nuclear fraction gave a positive signal with anti-CREB with undetectable levels of β-Tubulin or GAPDH (Fig. 4c; Supplementary Fig. 9b), indicating that the nuclear fraction was free of cytoplasmic contaminants. Having confirmed the purity of the isolated nuclear fraction, we probed the two fractions with anti-pan PKA RI, anti-PKA RIIβ and anti-PKA catalytic subunit antibodies. The nuclear fraction gave a positive signal for both PKA regulatory and catalytic subunits (Fig. 4c), providing direct evidence for the presence of PKA holoenzyme in the nucleus.

In order to link the nuclear PKA holoenzyme with the fast PKA responses in the nucleus, we used a mutant PC12 cell line deficient in nuclear PKA activity[24] (A126.1B2, Supplementary Fig. 10a). This mutant cell line has a significantly decreased level of PKA catalytic subunit in the nuclei[24] (Supplementary Fig. 10a), and stimulation with Fsk does not elicit a response of nuclear AKAR (Supplementary Fig. 10b). Because PKA RI subunit is still present in the

nuclei at a high level (Supplementary Fig. 10a), we tested if increasing the amount of catalytic subunit in the nucleus and thereby enriching the nuclear PKA holoenzyme pool would enable fast nuclear PKA responses. Indeed, Fsk-stimulation generated a fast nuclear AKAR response ($t_{1/2} = 2.9 \pm 0.3$ min; n = 2; Supplementary Fig. 10b), when NLS-tagged catalytic subunit (Cat-NLS) was overexpressed in A126.1B2. This rapid response was consistent with the kinetics of activation of the nuclear PKA holoenzyme predicted by the nucPKA model ($t_{1/2} = 6.1$ min) as well as the observed fast nuclear PKA dynamics when cAMP was produced in the nucleus ($t_{1/2} = 4.2 \pm 0.5$ min; n = 7). In contrast, A126.1B2 cells stably transfected with untargeted catalytic subunit gave slow AKAR-NLS responses to Fsk stimulation (Supplementary Fig. 10b). Collectively, this data suggests that fast nuclear PKA responses require locally activatable nuclear PKA holoenzyme.

PDE4 regulates PKA responses in the nucleus

Having established the presence and activation of nuclear PKA holoenzyme, we set out to identify the components that regulate nuclear PKA responses. It is well established that PDEs can shape cAMP gradients in specific cellular compartments by restricting cAMP diffusion[3]. To test the role of PDEs in the regulation of nuclear PKA responses, we treated HEK-293 cells with 3-isobytl-1-methylxanthine (IBMX), a non-selective PDE inhibitor, and monitored AKAR-NLS response upon tmAC activation by Fsk. Inhibition of PDEs with IBMX significantly accelerated the kinetics of Fsk-stimulated nuclear PKA activity as indicated by a decreased $t_{1/2}$ of 12.5 ± 2.1 min (n = 18). In 44% of these cells, a very fast response ($t_{1/2} = 3.1 \pm 1.2$ min; n = 8) was observed (Fig. 5a), matching the kinetics of the nuclear PKA holoenzyme activation that were experimentally determined ($t_{1/2} = 4.2 \pm 0.5$ min; n = 7) and those predicted by the nucPKA Model ($t_{1/2} = 6.1$ min). These results suggest a role for PDEs in limiting the activation of the endogenous nuclear PKA pool when cAMP is produced at the plasma membrane.

PDE3 and PDE4 have been identified as the two major subfamilies of PDEs expressed in HEK-293 cells[25]. To identify which PDE isoform regulates PKA responses in the nucleus, we treated the cells with Fsk in the presence of either milrinone, a PDE3 isoform-selective inhibitor, or rolipram, a PDE4 selective inhibitor. The rolipram/Fsk cocktail induced a fast AKAR-NLS response with a $t_{1/2}$ of 5.4 ± 2.14 min (n = 8) (Fig. 5B). Conversely, treatment with a milrinone/Fsk cocktail, induced a slow AKAR-NLS response (Supplementary Fig. 11a), similar to Fsk stimulation alone. This data suggests that PDE4 is the predominant isoform responsible for regulating PKA responses in the nucleus. To identify the individual PDE4 subfamilies that are potentially involved in regulating the PKA activity in the nucleus, we co-expressed catalytically inactive point mutants of PDE4B and PDE4D with AKAR-NLS in HEK-293 cells[18,26]. These catalytically-inactive mutants exert a dominant negative (dn) effect by dislodging the endogenous PDE4 isoforms from their appropriate anchor sites[18,26]. Fsk elicited an AKAR-NLS response that was slow in cells overexpressing either dnPDE4B1 or dnPDE4B2 but fast in cells overexpressing dnPDE4D3 (Supplementary Fig. 11b), suggesting that PDE4D3 could be playing a role in modulating PKA responses in the nucleus of HEK-293 cells.

In light of the PDE data, we hypothesized that PDE4 may play a role in negatively regulating the propagation of the cAMP signal from plasma membrane to nucleus. Thus we tested how PDE inhibition affects the response of ICUE3-NLS upon cAMP production at the plasma membrane. However, Fsk stimulation led to fast, saturated responses of ICUE3-NLS either in the presence or absence of PDE inhibition (Supplementary Fig. 11c), making it impossible to evaluate the role of PDEs in restricting the amount of cAMP that enters the nucleus. This data also presented a paradox: if cAMP generated at the plasma membrane accumulates fast in the nucleus and produces a maximal response from ICUE3 (which has a lower affinity for cAMP than PKA[27,28]), why are nuclear PKA holoenzymes not being activated by this pool of cAMP? Indeed, when the nucPKA model was refitted to all of the ICUE3 and AKAR responses, it predicted fast nuclear responses of PKA irrespective of where cAMP was synthesized (Fig. 5c), contradicting the experimental observations (Fig. 2).

AKAP regulates nuclear PKA activity dynamics

To understand how PDE4 may limit nuclear PKA activation despite adequate levels of cAMP that accumulate in the nucleus upon Fsk stimulation, we hypothesized that PDE4 may form a signaling complex with nuclear PKA holoenzyme. Such an arrangement may allow nuclear PDEs to degrade cAMP local to the nuclear PKA holoenzyme, therefore raising the cAMP activation threshold. The existence of AKAPPDE complexes has been documented[29]. For example, a peri-nuclear targeted AKAP (mAKAP) has been shown to tether PDE4 to the AKAP-PKA complex and modulate local cAMP levels[30]. We then inferred the existence of a subnuclear AKAP which may bring nuclear PKA holoenzyme in close proximity to PDEs.

To test the validity of this hypothesis, we modified the nucPKA Model by adding a phenomenological subnuclear AKAP compartment (`nucAKAP Model'). We assume all nuclear PKA holoenzyme resides in this subnuclear AKAP compartment and that the apparent PDE concentrations in this compartment are raised significantly by protein tethering. Refitting the nucPKA Model to each of the data sets (Supplementary Methods, Supplementary Fig. 12), we observed significant improvement in the model predictions for nuclear PKA dynamics. Specifically, while both the refitted Classical Model and the nucPKA Model failed to predict the differences in nuclear PKA dynamics in response to membrane and cytosolic cAMP generation (Fig. 5c), nuclear PKA response kinetics computed by the nucAKAP model matched the experimental kinetics, for the membrane cAMP production (nucAKAP Model $t_{1/2}$ = 20.1 min vs. experimental $t_{1/2}$ = 20.2 ± 3.0 min; n = 4) as well as for cytosolic cAMP generation (nucAKAP Model $t_{1/2}$ = 5.0 min vs. experimental $t_{1/2}$ = 3.5 ± 0.3 min; n = 9) (Fig. 5c). These simulations suggest that differences in nuclear PKA kinetics may be explained by differences in apparent cAMP concentration which is specified by AKAP-bound PDE4. In this scenario, cytosolic sAC_t stimulation may generate a much larger nuclear cAMP signal than membrane sAC_t or tmAC stimulation, driving activation of a nuclear AKAP-bound PKA pool.

We also simulated PKA activity in the membrane, cytosol and nucleus in response to Fsk in the absence or presence of IBMX for each of the three models (Fig. 5d). The nucAKAP

Model best captured the slow nuclear PKA response to Fsk ($t_{1/2}$ = 24.9 min vs. $t_{1/2}$ = 26.0 ± 1.6 min; n = 13) and accelerated nuclear PKA response to Fsk in the presence of IBMX ($t_{1/2}$ = 17.4 min vs. $t_{1/2}$ = 12.5 ± 2.1; n = 18). The computed AIC values for the Classical Model (AIC = 3.95), nucPKA Model (AIC = 5.81) and nucAKAP Model (AIC = −37.50) suggest that the nucAKAP Model best describes the responses of nuclear PKA in our experiments, significantly outweighing both the Classical and nucPKA Models in explaining the differences in nuclear PKA dynamics. The corresponding Akaike weights for these models were < 0.001 for both the Classical and nucPKA Models and > 0.999 for the nucAKAP Model indicating that both the Classical and nucPKA Models are incapable of explaining how PDE4 limits nuclear PKA responses to tmAC stimulation.

To test the predicted role of AKAP, we pre-incubated HEK293 cells expressing AKAR-NLS with St-Ht31, a peptide that blocks the interaction between PKA and AKAP[31]. This treatment is experimentally analogous to reducing the nucAKAP Model to the nucPKA Model, with the expectation that disruption of AKAP-PKA interaction should accelerate nuclear PKA activation since PKA is no longer localized in the same signaling microdomain as the AKAP-tethered PDEs. Upon stimulation with Fsk, we observed fast kinetics of AKAR-NLS with a $t_{1/2}$ of 7.6 ± 1.2 min (n = 14) (Fig. 5e), which were similar to that exhibited by AKAR-NLS upon PDE inhibition. In contrast, when cells were preincubated with a negative control peptide with a scrambled sequence (St-Ht31P) and then treated with Fsk, we observed the same slow AKAR response with a $t_{1/2}$ of 25.3 ± 1.8 min (n = 9) comparable to treatment with Fsk alone (Fig. 5f). Taken together, these results confirm an important role of AKAPs in regulating the nuclear PKA response and support our conceptual model of AKAP-tethered PDE4 and PKA in a nuclear signaling complex.

Discussion

The ability to both monitor and precisely manipulate levels of cAMP at different subcellular loci is important for fully understanding the role of compartmentalized cAMP signaling in cells. Towards this end, we describe a new method, SMICUS, for dictating the location, kinetics and magnitude of cAMP signal via manipulation of sAC using combined chemical and genetic controls. Using bicarbonate stimulation and washout, sAC-mediated cAMP production is under tight temporal control. Furthermore, we can also dictate where in the cell cAMP is being produced by using genetically encoded localization signals to target sAC_t subcellularly. Second messenger generation in microdomains, such as mitochondria and vesicles, as well as nanodomains like membrane rafts, is made possible since the site of cAMP generation is dictated by molecular targeting rather than light as in the case of photolytic uncaging of cAMP analogs[32]. Compared to the uncaging method, activation of sAC leads to more efficient generation of cAMP within the cell due to its catalytic nature. In addition, sAC has the potential for being expressed in tissues or in transgenic models for the study of cAMP signaling pathways in a multicellular context. More recently, light-sensitive adenylyl cyclases from *Euglena gracilis* and the soil bacteria *Beggiatoa* have been exploited to generate cAMP within the cell upon stimulation with light[33,34], although generation of cAMP in specific organelles has yet to be demonstrated by this method. These new approaches should allow for organelle-specific and efficient generation of cAMP under strict

temporal control, thereby enabling mechanistic dissection of the spatiotemporal regulation of cAMP signaling in specific subcellular compartments.

On the computational modeling front, we adopted a unique strategy of assaying model structures via parameter estimation to infer the regulatory structure of a cell signaling network. Mechanistic models are often presumed to contain an appropriate structure and are used as surrogates for an experimental system[35]. Here, we draw upon findings in information theory to directly infer and test different model structures when they are not fully known *a priori*[22]. While traditional approaches in systems biology seek to quantify known relationships or integrate large data sets[36], our approach here illustrates a relatively under-utilized, but important application for computational models in complementing experimental studies: providing quantitative evidence for selecting from directly competing hypotheses.

In this study, we combined SMICUS with live-cell imaging and mathematical modeling to investigate how cAMP signals are translated into nuclear PKA activity. By showing that in addition to the translocated catalytic subunit of PKA, there exists a functional pool of PKA holoenzyme that contributes to nuclear PKA signaling, we revise the existing dogma of cAMP-PKA signaling in the nucleus[1,5,9]. We provide the first set of quantitative evidence that this novel pool of nuclear PKA holoenzyme can be activated to produce fast responses in the nucleus. In addition, we form a new conceptual model for the regulation of nuclear PKA responses (Supplementary Fig. 13): the presence of an AKAP-mediated signaling complex that localizes PDE4 in close proximity to nuclear PKA holoenzyme largely controls nuclear PKA activity. When cAMP is generated at the plasma membrane and diffuses into the nucleus, local cAMP concentration in this nuclear PKA signaling domain is kept low by AKAP-anchored PDE4s and is not capable of efficiently activating nuclear PKA holoenzyme. As a result, nuclear PKA responses are characterized by slow kinetics, rate-limited by the translocation of the catalytic domain of cytosolic PKA. However, when the local cAMP concentration is elevated above a threshold, for example via activation of cytoplasmic- or nuclear-targeted sAC_t, activation of nuclear PKA holoenzyme can occur and generate fast kinetics of nuclear PKA responses. This nuclear PKA signaling domain assembled by AKAP therefore serves to manipulate the cAMP concentration threshold necessary to activate nuclear PKA holoenzyme in order to convert spatially distinct cAMP signals into temporal control of nuclear PKA activity. Future experiments will focus on identifying the responsible AKAP and characterizing the signaling complex. In addition, we will also evaluate the functional impact of such temporal control of nuclear PKA responses on processes such as transcription and RNA splicing as well as identify signaling sensing networks that are linked to this nuclear pool. A potential upstream component of nuclear PKA is endogenous sAC that has been suggested to exist in the nuclei of several cell types and produce cAMP in situ in response to changes in metabolic activities[11].

In summary, we combine targeted biochemical manipulation, real-time activity measurement and quantitative mechanistic modeling to provide evidence for the existence and distinct regulation of nuclear PKA holoenzyme. We propose a new model that localized negative regulators, in this case PDE4, help establish a local signaling threshold to convert spatial second messenger signals to temporal control of kinase activity. The quantitative

native biochemistry approach[17,37,38] utilized here should facilitate further testing of this model in this and other cell systems, leading to a better understanding of the mechanistic intricacies that underlie compartmentalized cAMP signaling.

Methods

Gene construction

sAC_t-NES fusion was generated by cloning the first 469 amino acids from rat sAC via PCR amplification using NcoI and SalI restriction sites for N and C termini and ligating it into pRSETB vector bacterial vector (Invitrogen). An internal BamHI site was silently mutated using QuikChange mutagenesis. mCherry with no stop codon was subcloned into the sAC_t-containing vector between SalI and EcoRI sites and the entire sequence was subcloned into a modified mammalian expression vector, pcDNA3 (Invitrogen), containing an NES sequence (5'-LPPLERLTL) at the C terminal end of the MCS using BamHI and EcoRI restriction sites. For NLS and PM targeting, sAC_tmCherry was subcloned into pcDNA3 vectors containing the sequences coding for 5'- PKKKRKVEDA at the C terminus between EcoRI and XbaI sites and 5'-GCIKSKRKDK at the N terminus between HindIII and BamHI sites, respectively.

Cell culture

HEK-293T cells were maintained in DMEM (10% FBS and 1% pen/strep) at 37°C with 5% CO_2. For imaging, cells were plated onto sterilized glass coverslips in 35-mm dishes and transfected with Lipofectamine2000 (Invitrogen) at 50–60% confluency and allowed to grow for 18–24 h before imaging.

Live-cell Imaging

Cells were washed twice with and maintained in Hanks' balanced salt solution buffer and allowed to equilibrate for 10 minutes in a CO_2 independent incubator. Cells were treated with $NaHCO_3$ (J.T.Baker, purity = 100%), KH7 (Cayman, purity   98%), Na_2HPO_4 (J.T.Baker, purity = 99.7%), forskolin (Fsk; Calbiochem, purity   99% by HPLC), IBMX (3-isobytl-1-methylxanthine; Sigma, purity   98% by TLC), rolipram (Alexis, purity   98% by TLC), milrinone (Alexis, purity   97% by TLC), St-Ht31P (Promega, purity > 80% by HPLC) and St-Ht31 (Promega, purity > 80% by HPLC) as indicated. Dual emission ratio imaging was performed on a Zeiss Axiovert 200M microscope with a MicroMAX BFT512 cooled charge-coupled device camera (Roper Scientific) controlled by METAFLUOR 6.2 software (Molecular Devices). Emission ratios were obtained using a 420DF20 excitation filter, a 450DRLP dichroic mirror, and two emission filters (475DF40 for cyan fluorescent protein and 535DF25 for yellow fluorescent protein present in ICUE3 and AKAR) alternated by Lambda 10–2 filter-changer (Sutter Instruments). RFP images were taken with a 568DF55 excitation filter, a 600DRLP dichroic mirror and a 653DF95 emission filter. Images were taken every 20s with an exposure time of 100–500ms. Fluorescent images were background-corrected by subtracting autofluorescence intensities of untransfected cells (or background with no cells) from the emission intensities of cells expressing reporters.

Model Construction

A computational model was developed to specifically describe cAMP and PKA dynamics in HEK-293 cells in MATLAB (Mathworks, Natick, MA). The final model consists of three spatial compartments (plasma membrane, cytosol, and nucleus) and one functional compartment (AKAP). Equations describing PKA activation by cAMP were based on work by Rich et al[39,40]. Equations describing ICUE3 and AKAR activity were based on Saucerman et al[41]. cAMP generated by endogenous and soluble adenylyl cyclases was permitted to freely diffuse across all compartments and activate PKA. Active PKA catalytic subunit was also permitted to diffuse across all compartments. PDE degradation of cAMP and AKAR regulation by PKA and phosphatases were described using Michaelis-Menten kinetics. Parameters for adenylyl cyclase activity, cAMP and PKA diffusion, PDE activity and phosphatase activity were estimated by nonlinear least squares fitting from randomized initial parameter sets, constrained by the magnitudes or $t_{1/2}$ values from corresponding ICUE3 and AKAR experimental measurements. For each simulation, the model was run to steady state before stimulation by Fsk, Fsk+IBMX or $NaHCO_3$. Simulations ran for 60 min, corresponding to the average length of the nuclear ICUE3 and AKAR experiments. A detailed description of the model equations and parameters are given in the Supplementary Methods.

Model Analysis

Comparisons between the suitability of the different model structures were made using the Akaike Information Criterion (AIC), an empirical estimate of the information given by a particular model structure[22,23]. The AIC rewards model agreement with fitted experimental data and penalizes addition of fit parameters. For the least squares case with a small sample size, the corrected AIC is given by

$$AIC = nlog\left(\frac{RSS}{n}\right) + 2K \cdot \frac{n}{n-K-1},$$

where n is the number of experimental measurements, RSS is the residual sum of squared errors and K is the number of model parameters. Within a set of fitted models, the "best model" minimizes the AIC. The probability that a given model within a set of models is most representative of a set of experimental data is given by the Akaike weight[22]:

$$w_i = \frac{exp\left(-1/2\Delta_i\right)}{\sum\limits_{r=1}^{R} exp\left(-1/2\Delta_r\right)},$$

where Δ_i is the difference between the AIC of the ith model with the minimum AIC from a set of R models. These Akaike weights are equivalent to the Bayesian posterior model probabilities and sum to 1 for any particular set of models.

Immunofluorescence

HEK-293T cells were fixed with 4% paraformaldehyde for 20 min, washed with DPBS, permeabilized with 0.2% Triton X-100 (Sigma), and incubated with pan PKA RI, PKA RIIβ and PKA catalytic α subunits (1:250 dilution for all three), followed by a 30 min incubation with Alexa Fluor546 conjugated goat anti-mouse secondary antibody (Invitrogen Molecular Probes). Cells were mounted with DAPI-containing medium and subjected to confocal imaging.

Nuclear fractionation

Sucrose buffers I and II for the fractionation were made as per protocol from Current Protocols in Molecular Biology[42]. HEK-293 cells were scraped, collected and spun at 1500 RPM for 10 min. The cell pellet was loosened by gentle vortexing for 5 sec and resuspended in 4 mL of ice-cold sucrose buffer I. After transferring to an ice-cold Dounce homogenizer, cells were lysed by 5–10 strokes of a B pestle. The lysate was removed to a 50 mL faclon tube and gently mixed with 4 mL of sucrose buffer II. This mixture was carefully layered onto a 4.4 mL cushion of sucrose buffer II in a polyallomer SW40.1 and the tube was filled to the top with sucrose buffer I. The Nuclear fraction was separated by centrifugation at 30,000×g for 45 minutes at 4°C using a Beckman centrifuge with a SW41Ti rotor. Both nuclear and non-nuclear fractions were probed with antibodies for CREB, tubulin, GAPDH, pan PKA RI, PKA RIIβ and PKA catalytic α subunits.

Statistical analysis

Unpaired t-tests were performed with Welch's correction using GraphPad Prism 4.03 (GraphPad Software). A P value of <0.05 was considered statistically significant.

Supplementary Material

Refer to Web version on PubMed Central for supplementary material.

Acknowledgements

Reference List

1. Tasken K, Aandahl EM. Localized effects of cAMP mediated by distinct routes of protein kinase A. Physiol Rev. 2004; 84:137–67. [PubMed: 14715913]

2. Steinberg SF, Brunton LL. Compartmentation of G protein-coupled signaling pathways in cardiac myocytes. Annual Review of Pharmacology and Toxicology. 2001; 41:751–773.

3. Houslay MD. Underpinning compartmentalised cAMP signalling through targeted cAMP breakdown. Trends Biochem Sci. 2010; 35:91–100. [PubMed: 19864144]

4. Carnegie GK, Means CK, Scott JD. A-kinase anchoring proteins: from protein complexes to physiology and disease. IUBMB Life. 2009; 61:394–406. [PubMed: 19319965]

5. Altarejos JY, Montminy M. CREB and the CRTC co-activators: sensors for hormonal and metabolic signals. Nat Rev Mol Cell Biol. 2011; 12:141–51. [PubMed: 21346730]

6. Kvissel AK, et al. Involvement of the catalytic subunit of protein kinase A and of HA95 in pre-mRNA splicing. Exp Cell Res. 2007; 313:2795–809. [PubMed: 17594903]

7. Martin BR, Deerinck TJ, Ellisman MH, Taylor SS, Tsien RY. Isoform-specific PKA dynamics revealed by dye-triggered aggregation and DAKAP1alpha-mediated localization in living cells. Chem Biol. 2007; 14:1031–42. [PubMed: 17884635]

8. Harootunian AT, et al. Movement of the free catalytic subunit of cAMP-dependent protein kinase into and out of the nucleus can be explained by diffusion. Mol Biol Cell. 1993; 4:993–1002. [PubMed: 8298196]

9. Mayr B, Montminy M. Transcriptional regulation by the phosphorylation-dependent factor CREB. Nat Rev Mol Cell Biol. 2001; 2:599–609. [PubMed: 11483993]

10. Meoli E, et al. Protein kinase A effects of an expressed PRKAR1A mutation associated with aggressive tumors. Cancer Res. 2008; 68:3133–41. [PubMed: 18451138]

11. Zippin JH, et al. Bicarbonate-responsive "soluble" adenylyl cyclase defines a nuclear cAMP microdomain. J Cell Biol. 2004; 164:527–34. [PubMed: 14769862]

12. Jarnaess E, et al. Splicing factor arginine/serine-rich 17A (SFRS17A) is an A-kinase anchoring protein that targets protein kinase A to splicing factor compartments. J Biol Chem. 2009; 284:35154–64. [PubMed: 19840947]

13. Steegborn C, Litvin TN, Levin LR, Buck J, Wu H. Bicarbonate activation of adenylyl cyclase via promotion of catalytic active site closure and metal recruitment. Nat Struct Mol Biol. 2005; 12:32–7. [PubMed: 15619637]

14. Chen Y, et al. Soluble adenylyl cyclase as an evolutionarily conserved bicarbonate sensor. Science. 2000; 289:625–8. [PubMed: 10915626]

15. Buck J, Sinclair ML, Schapal L, Cann MJ, Levin LR. Cytosolic adenylyl cyclase defines a unique signaling molecule in mammals. Proc Natl Acad Sci U S A. 1999; 96:79–84. [PubMed: 9874775]

16. DiPilato LM, Zhang J. The role of membrane microdomains in shaping beta2-adrenergic receptor-mediated cAMP dynamics. Mol Biosyst. 2009; 5:832–7. [PubMed: 19603118]

17. Ni Q, et al. Signaling diversity of PKA achieved via a Ca2+-cAMP-PKA oscillatory circuit. Nat Chem Biol. 2011; 7:34–40. [PubMed: 21102470]

18. Terrin A, et al. PGE(1) stimulation of HEK293 cells generates multiple contiguous domains with different [cAMP]: role of compartmentalized phosphodiesterases. J Cell Biol. 2006; 175:441–51. [PubMed: 17088426]

19. DiPilato LM, Cheng X, Zhang J. Fluorescent indicators of cAMP and Epac activation reveal differential dynamics of cAMP signaling within discrete subcellular compartments. Proc Natl Acad Sci U S A. 2004; 101:16513–8. [PubMed: 15545605]

20. Allen MD, Zhang J. Subcellular dynamics of protein kinase A activity visualized by FRET-based reporters. Biochem Biophys Res Commun. 2006; 348:716–21. [PubMed: 16895723]

21. Hagiwara M, et al. Coupling of hormonal stimulation and transcription via the cyclic AMP-responsive factor CREB is rate limited by nuclear entry of protein kinase A. Mol Cell Biol. 1993; 13:4852–9. [PubMed: 8336722]

22. Burnham, KP.; Anderson, DR. Model selection and multimodel inference : a practical information-theoretic approach. Springer; New York: 2002. p. xxvip. 488

23. Sugiura N. Further Analysis of Data by Akaikes Information Criterion and Finite Corrections. Communications in Statistics Part a-Theory and Methods. 1978; 7:13–26.

24. Shimojo M, Paquette AJ, Anderson DJ, Hersh LB. Protein kinase A regulates cholinergic gene expression in PC12 cells: REST4 silences the silencing activity of neuron-restrictive silencer factor/REST. Mol Cell Biol. 1999; 19:6788–95. [PubMed: 10490617]

25. Lynch MJ, et al. RNA silencing identifies PDE4D5 as the functionally relevant cAMP phosphodiesterase interacting with beta arrestin to control the protein kinase A/AKAP79-mediated switching of the beta2-adrenergic receptor to activation of ERK in HEK293B2 cells. J Biol Chem. 2005; 280:33178–89. [PubMed: 16030021]

26. McCahill A, et al. In resting COS1 cells a dominant negative approach shows that specific, anchored PDE4 cAMP phosphodiesterase isoforms gate the activation, by basal cyclic AMP

production, of AKAP-tethered protein kinase A type II located in the centrosomal region. Cell Signal. 2005; 17:1158–73. [PubMed: 15905070]

27. de Rooij J, et al. Mechanism of regulation of the Epac family of cAMP-dependent RapGEFs. J Biol Chem. 2000; 275:20829–36. [PubMed: 10777494]

28. Beavo JA, Bechtel PJ, Krebs EG. Activation of protein kinase by physiological concentrations of cyclic AMP. Proc Natl Acad Sci U S A. 1974; 71:3580–3. [PubMed: 4372627]

29. Wong W, Scott JD. AKAP signalling complexes: focal points in space and time. Nat Rev Mol Cell Biol. 2004; 5:959–70. [PubMed: 15573134]

30. Dodge-Kafka KL, et al. The protein kinase A anchoring protein mAKAP coordinates two integrated cAMP effector pathways. Nature. 2005; 437:574–8. [PubMed: 16177794]

31. Michel JJ, Scott JD. AKAP mediated signal transduction. Annu Rev Pharmacol Toxicol. 2002; 42:235–57. [PubMed: 11807172]

32. Ellis-Davies GC. Caged compounds: photorelease technology for control of cellular chemistry and physiology. Nat Methods. 2007; 4:619–28. [PubMed: 17664946]

33. Stierl M, et al. Light modulation of cellular cAMP by a small bacterial photoactivated adenylyl cyclase, bPAC, of the soil bacterium Beggiatoa. J Biol Chem. 2011; 286:1181–8. [PubMed: 21030594]

34. Schroder-Lang S, et al. Fast manipulation of cellular cAMP level by light in vivo. Nat Methods. 2007; 4:39–42. [PubMed: 17128267]

35. Kholodenko BN, Hancock JF, Kolch W. Signalling ballet in space and time. Nat Rev Mol Cell Biol. 2010; 11:414–26. [PubMed: 20495582]

36. Chuang HY, Hofree M, Ideker T. A decade of systems biology. Annu Rev Cell Dev Biol. 2010; 26:721–44. [PubMed: 20604711]

37. Tay S, et al. Single-cell NF-kappaB dynamics reveal digital activation and analogue information processing. Nature. 2010; 466:267–71. [PubMed: 20581820]

38. Paliwal S, et al. MAPK-mediated bimodal gene expression and adaptive gradient sensing in yeast. Nature. 2007; 446:46–51. [PubMed: 17310144]

39. Rich TC, et al. Cellular mechanisms underlying prostaglandin-induced transient cAMP signals near the plasma membrane of HEK-293 cells. Am J Physiol Cell Physiol. 2007; 292:C319–31. [PubMed: 16899551]

40. Xin W, Tran TM, Richter W, Clark RB, Rich TC. Roles of GRK and PDE4 activities in the regulation of beta2 adrenergic signaling. J Gen Physiol. 2008; 131:349–64. [PubMed: 18347080]

41. Saucerman JJ, et al. Systems analysis of PKA-mediated phosphorylation gradients in live cardiac myocytes. Proc Natl Acad Sci U S A. 2006; 103:12923–8. [PubMed: 16905651]

42. Greenberg ME, Bender TP. Identification of newly transcribed RNA. Curr Protoc Mol Biol. 2007; Chapter 4(Unit 4):10. [PubMed: 18265405]
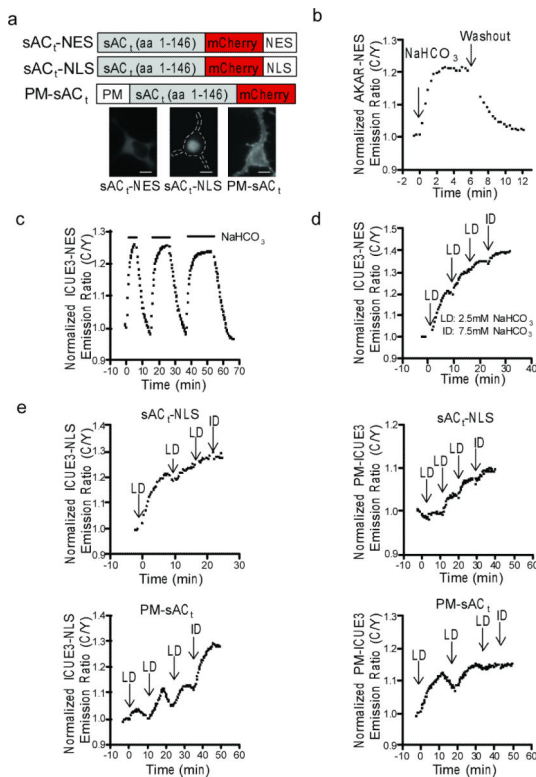
Figure 1. Spatiotemporal manipulation of intracellular cAMP using sAC (SMICUS) in HEK-293 cells

(a) Domain scheme of sAC_t-NES, sAC_t-NLS, and PM-sAC_t. RFP images of HEK-293 cells transiently transfected with the subcellularly targeted versions of sAC_t showing localization of sAC_t-NES to the cytoplasm, sAC_t-NLS to the nucleus and PM-sAC_t to the plasma-membrane. Scale bars, 10 μm. (b) Representative time course of yellow/cyan (Y/C) emission ratio changes in single HEK-293 cells expressing AKAR-NES and sAC_t-NES showing that sAC_t-NES mediated cAMP production can be reversed upon washout (n = 5). (c) Response of ICUE3-NES to repeated stimulation and washout. There is no detectable desensitization of the system. (d) The amplitude of ICUE3-NES responses can be tuned with the addition of low doses (LD) of 2.5 mM and intermediate doses (ID) of 7.5 mM $NaHCO_3$ (n = 3). (e) Top panel: Representative response curves of ICUE3-NLS (left; n = 5) and PM-ICUE3 (right; n = 2) upon stimulation of sAC_t-NLS. Bottom panel: ICUE3-NLS (left; n = 3) and PM-ICUE3 (right; n = 2) with activation of PM-sAC_t demonstrating that SMICUS can be used to tune local cAMP signals.
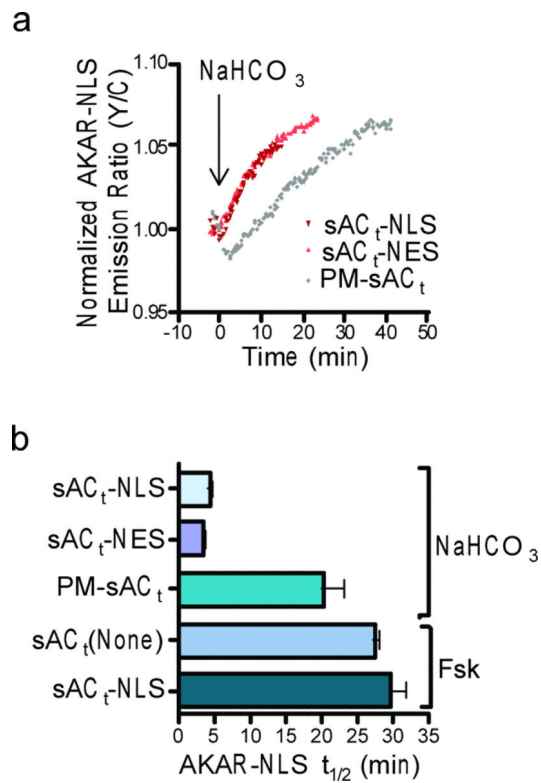
Figure 2. Spatial manipulation of cAMP production reveals differential PKA activity dynamics in the nuclei of HEK-293 cells

(a) Representative response curves for AKAR-NLS upon 15 mM $NaHCO_3$ stimulation of sAC_t-NLS (red inverted triangle; n = 7), sAC_t-NES (orange triangle; n = 9) and PM-sAC_t (gray diamond; n = 4). (b) Comparison of $t_{1/2}$ values reveals statistically significant differences in PKA kinetics mediated by membrane- versus cytosol/nuclear-generated cAMP. All data are presented as average ± SEM.
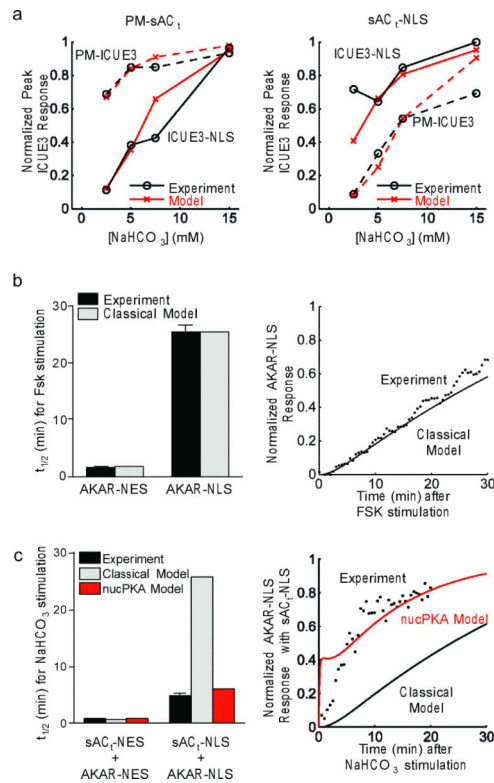
Figure 3. Rapid nuclear PKA responses to local cAMP accumulation require nuclear PKA holoenzyme

(a) Classical Model fits to local and distal ICUE responses to $NaHCO_3$-stimulated cAMP production by membrane (left) and nuclear (right) sACs. (b) Left: Classical Model fit to AKAR responses to 50 μM Fsk in the cytosol and nucleus. Right: Time course depiction of Classical Model fit to nuclear PKA activation by 50 μM Fsk. (c) Left: Classical Model and nucPKA Model fit to local AKAR responses to local sAC stimulation by 15 mM $NaHCO_3$. Right: Time course depictions of Classical Model and nucPKA Model fits to nuclear PKA activation by nuclear sAC stimulation. nucPKA Model differs from the Classical Model only by addition of nuclear PKA holoenzyme.
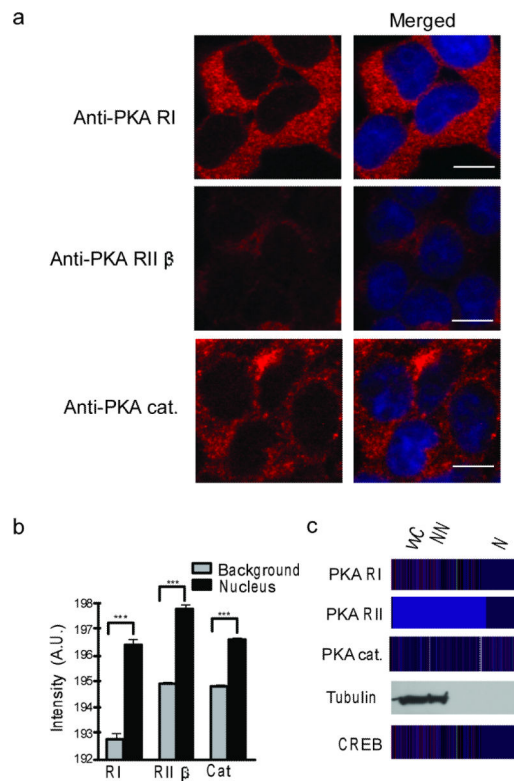
Figure 4. PKA holoenzyme is in the nuclei of HEK-293 cells

(a) Immunofluorescence staining using anti-pan RI PKA, RIIβ PKA and Cα PKA antibodies gave a detectable signal in the nuclei of HEK-293 cells. Nuclei were stained with DAPI, a blue-fluorescent nucleic acid marker. Scale bars, 10 μm. (b) A graphical representation of the intensities in Arbitrary Unit (A.U.) comparing the signal in the nuclei to the background for each antibody staining (P<0.0001 for all three) (c) Immunoblot analysis was carried out on whole cell (WC), non-nuclear (NN) and nuclear (N) fractions with anti-pan RI PKA, RIIβ PKA and Cα PKA antibodies. Probing with anti-tubulin and anti-CREB antibodies showed that the nuclear fraction was free of cytosolic proteins (see Supplementary Fig. 14 for full blots).
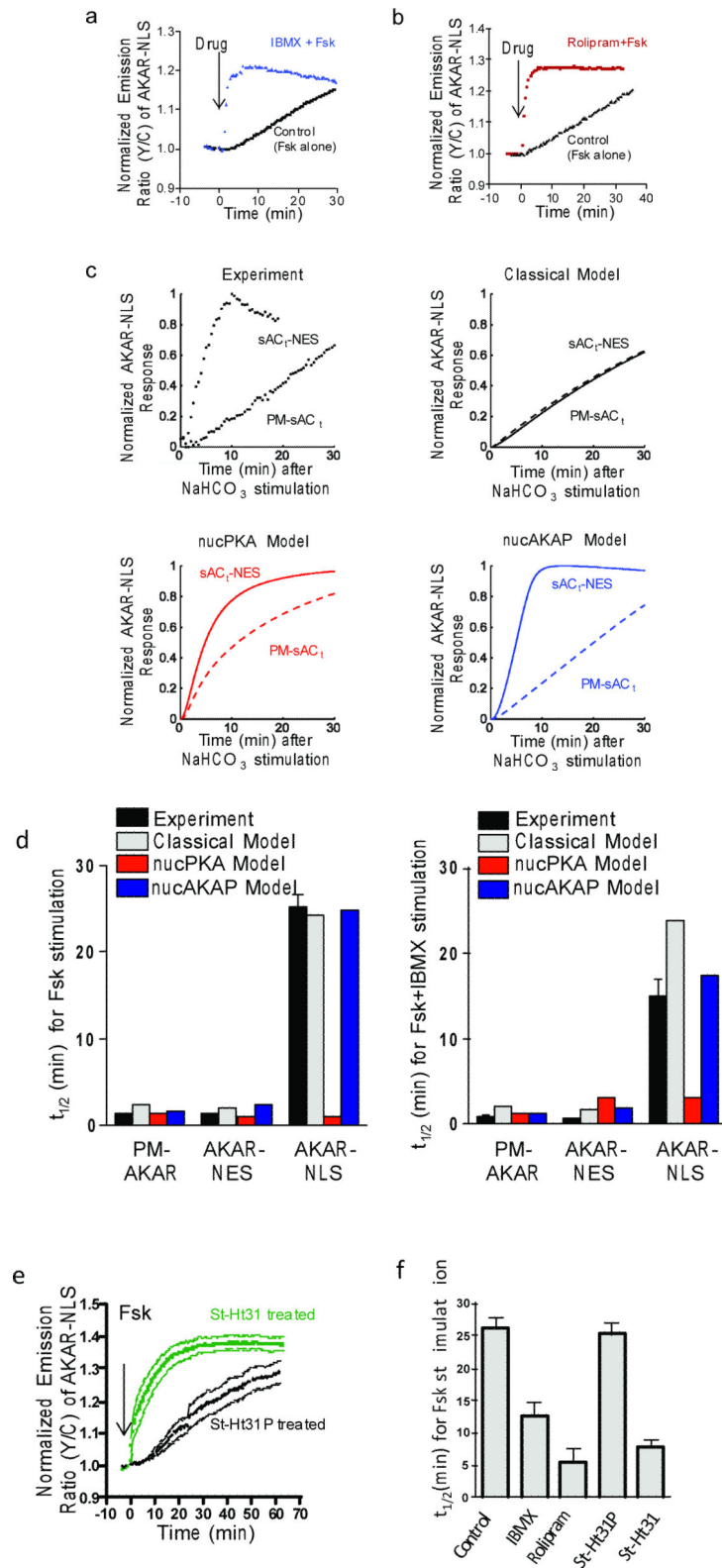
Figure 5. cAMP-PKA signaling in the nuclei of HEK-293 cells is tightly regulated by PDEs and AKAPs

(a) PDE inhibition by 100 μM IBMX accelerated AKAR-NLS kinetics upon tmAC activation by 50 μM Fsk (representative blue curve; n = 18) compared against slow nuclear PKA responses to 50 μM Fsk alone in control cells (representative grey curve; n=13). (b) Co-treatment with 10 μM Rolipram, a PDE4 specific inhibitor, and Fsk results in faster AKAR-NLS responses (representative red curve; n = 8) compared to Fsk stimulation alone (representative black curve; n = 13). (c) Simulated time course comparisons between the Classical, nucPKA and nucAKAP models for predicting slow and fast nuclear PKA responses to membrane cAMP generation and cytosolic cAMP generation, respectively (representative experimental time course depicted). (d) Classical, nucPKA and nucAKAP Model fits to compartmented PKA kinetics in response to 50 μM Fsk in the absence (left) or presence of 100 μM IBMX (right). The nucAKAP Model best captures both the slow response to 50 μM Fsk alone and the marked acceleration by IBMX addition. (e) Disruption of PKAAKAP interaction with 50 μM St-Ht31 (green curve, averaged responses (n = 14)) results in a rapid AKAR-NLS response upon Fsk stimulation while treatment with St-Ht31P (scramble control, black curve, averaged responses (n = 9)) has no effect on Fsk-stimulated AKAR-NLS response. (f) Measured nuclear AKAR $t_{1/2}$s indicate PDE inhibition and AKAP disruption are both sufficient for accelerating nuclear PKA responses.